Phonon Dichroisms Revealing Unusual Electronic Quantum Geometry

Ding Li,^{1,2,*} Guoao Yang,^{3,1,*} Tao Qin,^{3,†} Jianhui Zhou,^{1,‡} and Yugui Yao^{4,5,§}

¹Anhui Provincial Key Laboratory of Low-Energy Quantum Materials and Devices,
High Magnetic Field Laboratory, HFIPS, Chinese Academy of Sciences, Hefei, Anhui 230031, China
²Department of Physics, University of Science and Technology of China, Hefei 230026, P.R. China
³School of Physics and Optoelectronics Engineering,
Anhui University, Hefei, Anhui Province 230601, P.R. China
⁴Centre for Quantum Physics, Key Laboratory of Advanced Optoelectronic Quantum Architecture and Measurement,

⁴Centre for Quantum Physics, Key Laboratory of Advanced Optoelectronic Quantum Architecture and Measureme School of Physics, Beijing Institute of Technology, Beijing 100081, China ⁵Beijing Key Lab of Nanophotonics and Ultrafine Optoelectronic Systems, School of Physics, Beijing Institute of Technology, Beijing 100081, China

The quantum geometry tensor, intrinsic geometric characteristics of electronic states, plays a crucial role in the various nontrivial electromagnetic phenomena in quantum materials. Here, we reveal that quantum geometry significantly modifies phonon dichroisms through electron-phonon interactions in solids that break time-reversal and spatial inversion symmetries. Specifically, the circular phonon dichroism is primarily dominated by the heat magnetic moments, while the linear phonon dichroism depends on the heat Drude weight, a thermal analog of band Drude weight. Furthermore, we establish the f-sum rule for the heat magnetic moment that facilitates its experimental detections. We demonstrate our key findings in an archetypal model system: ferromagnetic two-dimensional electron gases with Rashba spin-orbit coupling. Our work uncovers the quantum-geometric origin of common phonon dichroisms and predicts the detectable signature of the heat magnetic moment of electrons in solids.

Introduction.--The familiar quantum geometry tensor characterizes the fundamental geometric properties of nearby quantum states in Hilbert space, whose imaginary part and real part correspond to the Berry curvature and quantum metric, respectively [1-3]. The Berry curvature modifies the electronic properties through an anomalous velocity, which has played a vital role in understanding various dissipation-less quantum effects [4, 5] and the emergence of the topological phases of matter [6-8]. Recently, the quantum metric has also manifested in a plenty of fundamental phenomena in quantum materials [9–18], such as the nonlinear Hall effect [19–21]. However, the quantum geometry effect in the electroncollective excitation (such as phonon, plasmon, magnon) coupled systems in conducting crystals remains largely elusive [22, 23].

Controllable symmetry breaking of crystal primarily determines the essential behaviors of quantum geometry tensor and the resulting quantum phenomena [4, 5]. For example, the nontrivial Berry curvature in the momentum space requires the breaking of either time reversal or spatial inversion symmetry. The Berry curvature leads to the self-rotation of wave packet of Bloch electrons which is accompanied with orbital magnetic moment [24, 25] and heat magnetic moment (HMM) of electrons [26]. Remarkably, the orbital magnetic moment is closely related to the dynamical Hall responses and can be effectively probed by the magnetic circular dichroism [27–33]. Nevertheless, the manifestation, detection and manipulation of HMM of electrons are still challenging, a prime reason is the lack of independent and easily accessible quantum phenomena dominated by the HMM of electrons. Here we focus on the key roles of quantum

geometry in phonon dichroisms (the differential absorption of linearly or circularly polarized phonons) through the electron-phonon coupling, allowing the current-free, contactless and acoustic detection of HMM of electrons.

In this work, we uncover the intimate connection between unusual electronic quantum geometry and phonon dichroism. Specifically, the circular phonon dichroism is predominately driven by the HMMs of electrons, while the linear phonon dichroism originates from the heat Drude weight. We derive the f-sum rule of HMM to facilitate experimental detections, in analogy to the orbital magnetization. Moreover, we demonstrate our key findings in the representative ferromagnetic two-dimensional electron gases (2DEG) with Rashba spin-orbit coupling (SOC) and brief its experimental detections.

Formalism of phonon dichroisms.--We start from the equation of motion for ions in metals:

$$\omega^{2} u_{\alpha} (\mathbf{q}) = \sum_{\beta} \left(\hbar^{2} \Phi_{\alpha\beta} (\mathbf{q}) + \hbar \chi_{\alpha\beta} (\mathbf{q}, \omega) \right) u_{\beta} (\mathbf{q}), \quad (1)$$

where $\hbar\omega$ is the phonon energy, $u_{\alpha}(\mathbf{q})$ is the Fourier transform of the displacement field along the α th direction $u_{\alpha}(\mathbf{r})$, and $\Phi_{\alpha\beta}(\mathbf{q})$ is the dynamic matrix. $\chi_{\alpha\beta}(\mathbf{q},\omega)$ is the retarded force-force response function [34]

$$\chi_{\alpha\beta}(\boldsymbol{q},\omega) = \sum_{n,n'} \int \frac{\hbar d^2 \boldsymbol{k}}{\rho(2\pi)^2} F_{n'n}(\omega,\boldsymbol{k},\boldsymbol{q}) S_{nn'}^{\alpha\beta}(\boldsymbol{k},\boldsymbol{q}), \quad (2)$$

where ρ is the 2D mass density, the dynamical factor becomes $F_{n'n}(\omega, \mathbf{k}, \mathbf{q}) = \frac{f_{n,n'}(\mathbf{k}, \mathbf{k'})}{\hbar\omega + i\delta + \varepsilon_{nn'}(\mathbf{k}, \mathbf{k} + \mathbf{q})}$ with the energy difference $\varepsilon_{mn}(\mathbf{k}, \mathbf{k'}) \equiv \varepsilon_m(\mathbf{k}) - \varepsilon_n(\mathbf{k'})$ and the

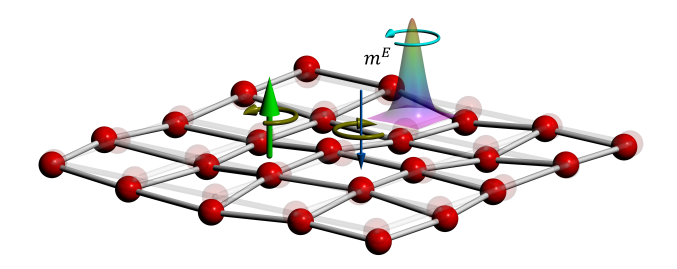


Figure 1. Schematic of the magnetic circular dichroism via electron-phonon coupling due to the the heat magnetic moments (\boldsymbol{m}^E) of the self-rotating electronic wave packet. The light and solid atoms indicate the lattice vibration. The green up (blue down) arrow refers to the absorptions of the right (left) circularly polarized phonons. The sizes of arrows indicate different strength of absorptions.

distribution-function difference $f_{n,n'}(\mathbf{k}, \mathbf{k}') \equiv f_n(\mathbf{k}) - f_{n'}(\mathbf{k}')$. $S_{nn'}^{\alpha\beta}(\mathbf{k}, \mathbf{q})$ is the product of the matrix elements of the force operator $\hat{T}_{\alpha}(\mathbf{q}) = -\partial \hat{H}_{e-ph}/\partial u_{\mathbf{q}\alpha}$ [35]

$$S_{nn'}^{\alpha\beta}(\mathbf{k}, \mathbf{q}) = \left\langle \psi_n(\mathbf{k}) | \hat{T}_{\alpha}(-\mathbf{q}) | \psi_{n'}(\mathbf{k} + \mathbf{q}) \right\rangle \times \left\langle \psi_{n'}(\mathbf{k} + \mathbf{q}) | \hat{T}_{\beta}(\mathbf{q}) | \psi_n(\mathbf{k}) \right\rangle, \tag{3}$$

which encodes the intrinsic geometric information of quantum states during the electron excitations by phonons, dubbed quantum geometric factor. Here n is the energy band index and $f_n(\mathbf{k})$ is the Fermi distribution function. $\varepsilon_n(\mathbf{k})$ denotes the energy dispersion of Bloch states $|\psi_n(\mathbf{k})\rangle$.

In order to describe the dissipation of phonons, we introduce a quantity $\gamma=\frac{i}{4\omega}(\chi-\chi^\dagger)$ as

$$\gamma = \begin{bmatrix} \gamma_{xx} & \gamma_{xy} \\ \gamma_{yx} & \gamma_{yy} \end{bmatrix} \tag{4}$$

with $\gamma_{\alpha\beta}(\boldsymbol{q},\omega) = \frac{-1}{2\omega} \sum_{n,n'} \int \frac{\hbar d^2 \boldsymbol{k}}{\rho(2\pi)^2} \mathrm{Im}[F_{n'n}(\omega,\boldsymbol{k},\boldsymbol{q})] \times S_{nn'}^{\alpha\beta}(\boldsymbol{k},\boldsymbol{q})$. We define $\gamma_D = (\gamma_{xx} + \gamma_{yy})/2$ and $\gamma_{\bar{D}} = (\gamma_{xx} - \gamma_{yy})/2$, which refer to the longitudinal absorptions, and furthermore, introduce $\gamma^A = \mathrm{Im}[\gamma_{xy}]$, related to the anomalous Hall absorption, and $\gamma^{\bar{A}} = \mathrm{Re}[\gamma_{xy}]$. For the linearly polarized longitudinal and transverse phonons $(\omega_{l/t} = c_{l/t} |\boldsymbol{q}|)$, the absorption coefficients are given by

$$\gamma^{l/t} = \gamma_D \pm \cos 2\phi_q \gamma_{\bar{D}} \pm \sin 2\phi_q \gamma^{\bar{A}}, \tag{5}$$

with $\phi_q = \tan^{-1}(q_y/q_x)$ [36], where \boldsymbol{q} is the phonon wave vector and $c_{l/t}$ is the phonon velocity. For the left- and right-hand circularly polarized phonons $\left(\frac{1}{2}\left(1,\pm i\right)^T\right)$, the absorption coefficients are given by $\gamma^{L/R} = \gamma_D \mp \gamma^A$. The difference between γ^l and γ^t defines the linear phonon dichroism, while the difference between γ^L and γ^R causes the circular phonon dichroism $(\gamma^A \equiv (\gamma^R - \gamma^L)/2)$ (see Fig. 1 for the schematic of its detection).

	Real	Imaginary
$\mathcal{F}_{nlphaeta}$	quantum metric	Berry curvature
	$g_{nlphaeta}$	$\Omega_{nlphaeta}$
$\mathcal{G}_{nlphaeta}$	band Drude weight	orbital magnetic moment
	$D_{n\alpha\beta}$	$m_{nlphaeta}$
$\mathcal{H}_{n\alpha\beta}$	heat Drude weight	heat magnetic moment
	$D_{n\alpha\beta}^{E}$	$m^E_{nlphaeta}$

Table I. Sestet of quantum geometric quantities associated with $\mathcal{F}_{n\alpha\beta}$, $\mathcal{G}_{n\alpha\beta}$ and $\mathcal{H}_{n\alpha\beta}$ of Bloch electrons. The real and imaginary parts of the quantum geometric tensors correspond to the symmetric part and antisymmetric part, respectively.

Quantum-geometric origin.--In order to uncover the clear quantum-geometric origin of phonon dichroisms, we consider a generic two-band model

$$H = d_0(\mathbf{k}) + \mathbf{d}(\mathbf{k}) \cdot \boldsymbol{\sigma}, \tag{6}$$

where the Pauli matrix σ_i could denote the real spin and pseudospin degree of freedom (such as lattice, orbit, layer) in the context of graphene [37], monolayer transition metal dichalcogenides [38, 39], the Rashba 2DEG [40, 41], Weyl semimetals [42] and topological surface states [43]. Without loss of generality, we assume that d_i are the polynomial function of k_x and k_y . Before proceeding, we should brief the six quantum geometric quantities (See Table. I). They can be expressed in terms of the unit vector $\hat{\mathbf{d}} \equiv \mathbf{d}/|\mathbf{d}|$ with $|\mathbf{d}| = \sqrt{d_1^2 + d_2^2 + d_3^2}$:

$$\mathcal{F}_{n\alpha\beta}(\mathbf{k}) = \mathcal{G}_{n\alpha\beta}(\mathbf{k})/2|\mathbf{d}| = \mathcal{H}_{n\alpha\beta}(\mathbf{k})/4|\mathbf{d}|^2, \quad (7)$$

where the conventional quantum geometry tensor is given as $\mathcal{F}_{n\alpha\beta}(\mathbf{k}) = g_{n\alpha\beta}(\mathbf{k}) - \frac{i}{2}\Omega_{n\alpha\beta}(\mathbf{k}), g_{n\alpha\beta}(\mathbf{k}) = \left(\partial_{\alpha}\hat{d}_{n} \cdot \partial_{\beta}\hat{d}_{n}\right)/4$ and $\Omega_{n\alpha\beta}(\mathbf{k}) = \hat{d}_{n} \cdot \left(\partial_{\alpha}\hat{d}_{n} \times \partial_{\beta}\hat{d}_{n}\right)/2$ respectively correspond to the quantum metric and Berry curvature of electrons [4, 44]. The real and imaginary part of $\mathcal{G}_{n\alpha\beta} \equiv D_{n\alpha\beta} - im_{n\alpha\beta}$ are associated with the band Drude weight and orbital magnetic moment [45, 46]. It is worth mentioning that the imaginary part of $\mathcal{H}_{n\alpha\beta} \equiv D_{n\alpha\beta}^E - im_{n\alpha\beta}^E$ refers to the HMM of electrons [26], while the real part could be regarded as the generalized heat Drude weight, in analogy to the band Drude weight in electric conductivity [47] (Details in the Supplemental Material [35]). In fact, the significance of the unusual quantum geometric tensor $\mathcal{H}_{n\alpha\beta}$ is rarely discussed before.

The electron-phonon coupling H_{e-ph} can be modeled by coupling the momentum with the local frame field e^{μ}_{j} via $p_{j} \rightarrow p_{\mu}e^{\mu}_{j}$, where $e^{\mu}_{j} = \delta^{\mu}_{j} - \partial u_{j} (\mathbf{r}) / \partial r_{\mu}$ describes the local stretching and rotation of lattice structure [48–50], and summation over repeated indices is implied henceforth. We further expand the factor $S^{\alpha\beta}_{nn'}(\mathbf{k},\mathbf{q})$ with respect to q to third order and have (Details are given in the Supplemental Material [35]) the intraband part

$$S_n^{\alpha\beta}(\boldsymbol{k},\boldsymbol{q})$$

$$= \frac{1}{2} \left(1 + \frac{1}{2} \boldsymbol{q} \cdot \boldsymbol{\nabla}_{k} \right) \left[\left(\boldsymbol{q} \cdot \boldsymbol{k} \right)^{2} v_{n\boldsymbol{k}}^{\alpha} v_{n\boldsymbol{k}}^{\beta} \right]$$

$$+ \left(\boldsymbol{q} \cdot \boldsymbol{k} \right)^{2} i q_{\nu} \operatorname{Im} \left[v_{n\boldsymbol{k}}^{\alpha} \mathcal{G}_{n\nu\beta} \left(\boldsymbol{k} \right) + v_{n\boldsymbol{k}}^{\beta} \mathcal{G}_{n\alpha\nu} \left(\boldsymbol{k} \right) \right]$$
(8)

and the interband part

$$S_{nm}^{\alpha\beta}(\mathbf{k}, \mathbf{q})$$

$$= \left(1 + \frac{1}{2}\mathbf{q} \cdot \nabla_{k}\right) \left[(\mathbf{q} \cdot \mathbf{k})^{2} \mathcal{H}_{n\mathbf{k}}^{\alpha\beta} \right]$$

$$+ (\mathbf{q} \cdot \mathbf{k})^{2} q_{\nu} \left[v_{nm\mathbf{k}}^{\alpha} \mathcal{G}_{n\nu\beta} (\mathbf{k}) + v_{mn\mathbf{k}}^{\beta} \mathcal{G}_{n\alpha\nu} (\mathbf{k}) \right]$$
(9)

where $v_{mnk}^{\alpha} \equiv \frac{1}{2} \left(v_{mk}^{\alpha} + v_{nk}^{\alpha} \right)$ is the mean velocity of two bands and will disappear for the particle-hole symmetric bands. Note that summation over repeated indices is assumed. According to the definition of γ matrix in Eq. (4), the linear phonon dichroism in Eq. (5) can be written as the leading-order contribution (up to q^2)

$$\gamma^{\bar{A}} = \frac{-\hbar}{2\omega\rho} \int \frac{d^2\mathbf{k}}{(2\pi)^2} (\mathbf{q} \cdot \mathbf{k})^2 \left\{ \frac{1}{2} \sum_{n} f_{n,n} (\mathbf{k}, \mathbf{k} + \mathbf{q}) \right.$$
$$\left. \times v_{n\mathbf{k}}^x v_{n\mathbf{k}}^y \delta \left[\varepsilon_{nn} (\mathbf{k} + \mathbf{q}, \mathbf{k}) - \hbar\omega \right] + \sum_{n \neq n'} D_{nxy}^E (\mathbf{k}) \right.$$
$$\left. \times f_{n,n'} (\mathbf{k}, \mathbf{k} + \mathbf{q}) \delta \left[\varepsilon_{n'n} (\mathbf{k} + \mathbf{q}, \mathbf{k}) - \hbar\omega \right] \right\}$$
(10)

and the diagonal element,

$$\gamma_{\alpha\alpha} = \frac{-\hbar}{2\omega\rho} \int \frac{d^2\mathbf{k}}{(2\pi)^2} (\mathbf{q} \cdot \mathbf{k})^2 \left\{ \frac{1}{2} \sum_n f_{n,n} (\mathbf{k}, \mathbf{k} + \mathbf{q}) \right.$$
$$\left. \times (v_{n\mathbf{k}}^{\alpha})^2 \delta \left[\varepsilon_{nn} (\mathbf{k} + \mathbf{q}, \mathbf{k}) - \hbar\omega \right] + \sum_{n \neq n'} D_{n\alpha\alpha}^E (\mathbf{k}) \right.$$
$$\left. \times f_{n,n'} (\mathbf{k}, \mathbf{k} + \mathbf{q}) \delta \left[\varepsilon_{n'n} (\mathbf{k} + \mathbf{q}, \mathbf{k}) - \hbar\omega \right] \right\}$$
(11)

where $D_{nxy}^{E}(\mathbf{k})$ is the heat Drude weight of electrons in the nth band and can be regarded as the cousin of the quantum metric with $\alpha = x, y$. It can be seen that the linear phonon dichroism is controlled by the quantum metric (See the full expressions of $\gamma^{\bar{A}}$ and $\gamma_{\alpha\alpha}$ [35]).

Let us turn to the circular phonon dichroism. Remarkably, the leading-order term quadratic in q of Im $\begin{bmatrix} S_{nm}^{\alpha\beta} \end{bmatrix}$ is directly related to the HMM of electrons from $\mathcal{H}_{nk}^{\alpha\beta}$ in Eq. (9) and leads to a basic and useful relation of the circular phonon dichroism

$$\gamma^{A}(\mathbf{q},\omega) \approx -\frac{\pi\hbar}{4\omega\rho} \sum_{n\neq n'} \int \frac{d^{2}\mathbf{k}}{(2\pi)^{2}} (\mathbf{q} \cdot \mathbf{k})^{2} m_{n\mathbf{k}}^{E} \times f_{n,n'}(\mathbf{k},\mathbf{k}+\mathbf{q}) \delta \left[\varepsilon_{n'n} (\mathbf{k}+\mathbf{q},\mathbf{k}) - \hbar\omega\right],$$
(12)

where $m_{n\mathbf{k}}^E$ is the HMM of electrons and the factor of $q^2/\omega\rho$ corresponds to the square of strength of electronphonon interaction [51].

In order to gain the fundamental quantities of electronic states, it is quite instructive to investigate the

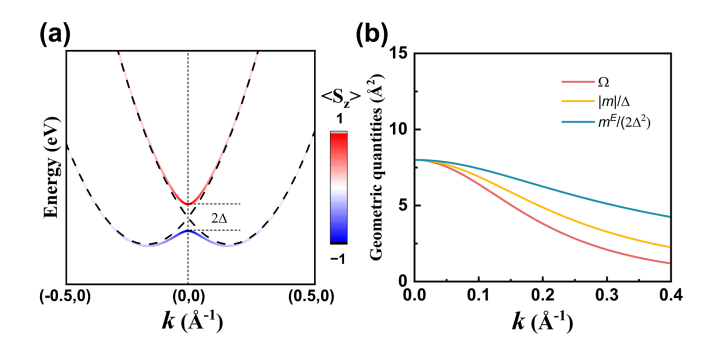


Figure 2. (a) The energy band of Rashba 2DEG in the presence (colored solid lines) or absence (dashed line) of out-ofplane Zeeman fields. (b) The corresponding radial distribution of the three quantum geometric quantities: Berry curvature, orbital magnetic moment and HMM of the E_- band.

sum rule [52]. In analogy to the well-known f-sum rule for the particle density, we consider a proper integral of $\gamma^A(\mathbf{q},\omega)\omega$ over ω as $I_{\gamma^A} \equiv \int \omega \gamma^A(\mathbf{q},\omega) d\omega$,

$$I_{\gamma^{A}} \approx -\frac{\pi\hbar}{4\rho} q_{\alpha\beta} \sum_{n \neq n'} \int \frac{d^{2}\mathbf{k}}{(2\pi)^{2}} k_{\alpha} k_{\beta} m_{n\mathbf{k}}^{E} f_{n,n'} \left(\mathbf{k}, \mathbf{k} + \mathbf{q}\right). \tag{13}$$

with $q_{\alpha\beta} \equiv (q_x^2, 2q_xq_y, q_y^2)$. In order to unravel the clean physical picture, we consider the particle-hole symmetric bands at low temperatures [53]. For simplicity, we set $\mathbf{q} = (q_x, q_y)$ is small relative to the Fermi vector k_F and the Fermi level lies in the valence band. Thus, the integration I_{γ^A} could be further simplified and becomes

$$I_{\gamma^A} \approx -\frac{\pi\hbar}{4\rho} q_{\alpha\beta} \sum_{\mathbf{r}} \int \frac{d^2 \mathbf{k}}{(2\pi)^2} k_{\alpha} k_{\beta} f_n(\mathbf{k}) m_{n\mathbf{k}}^E$$
 (14)

The right hand side of Eq. (14) is the sum of quadrupole of m_{nk}^E of filled states. It shows clearly that the circular phonon dichroism is primarily determined by m_{nk}^E of electrons. This formula provides a guiding principle to detect the HMM of electrons in experiments [54], similar to the magnetic circular dichroism of light or X-ray for the orbital magnetization in magnetic materials [55]. Eqs. (12)-(14) are central results of the present work. Next we would demonstrate the significance of quantum metric and HMM in phonon dichroisms in a typical quantum material.

Rashba 2DEG.--We first consider the generic 2DEG with Rashba SOC in the presence of an out-of-plane Zeeman field that can well describe the electrons at the surface of metals [40], LaAlO₃/SrTiO₃ oxide heterointerfaces [56] and KTaO₃-based heterostructures [57]. It acts as a model system for investigation of low-dissipation electromagnetic responses [41, 58, 59], chiral spin textures [60] and topological superconductivity [61]. The model is given as

$$H(\mathbf{k}) = tk^2 + \Delta\sigma_z + \lambda(k_x\sigma_y - k_y\sigma_x),\tag{15}$$

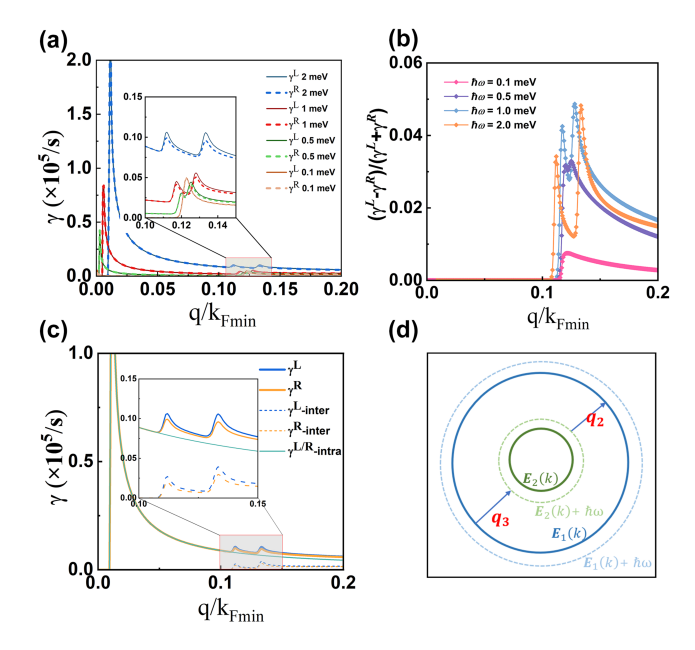


Figure 3. (a)-(d) Damping coefficients of $\gamma^{R/L}$ phonon modes versus the phonon wave-vector \boldsymbol{q} of Rashba 2DEG. (a) \boldsymbol{q} -dependence of $\gamma^{R/L}$ at several typical energies and $k_{Fmin} = \sqrt{(\mu - \Delta)/t}$. Insert shows the region for evident difference and γ^R and γ^L . (b) Two-peak signature in ratio of $(\gamma^L - \gamma^R)/(\gamma^R + \gamma^L)$ at phonon energies of $\hbar\omega = 0.5, 1.0$ meV. (c) Decomposition of strength of circular phonon dichroism in terms of the interband and intraband processes. (d) Origin of two-peak structure in the damping coefficients of $\gamma^{R/L}$. We fixed \boldsymbol{q} at a direction $\arctan(q_y/q_x) = \pi/4$ and q > 0. $\mu = 0.1$ eV is relative to the band bottom.

where t breaks particle-hole symmetry and Δ breaks time-reversal symmetries and gives rise to a band gap 2Δ at the Γ point (Fig. 2(a)) and $k = \sqrt{k_x^2 + k_y^2}$. Importantly, the Rashba SOC λ breaks the spatial inversion symmetry and is vital to the emergence of nontrivial quantum geometry tensors in momentum space. Some manipulations lead to the Berry curvature of the two bands $(E_{\pm} = tk^2 \pm \sqrt{\Delta^2 + \lambda^2 k^2}), \ \Omega_{\pm}^{xy}(\mathbf{k}) =$ $\frac{\mp\lambda^2\Delta}{2(\Delta^2+k^2\lambda^2)^{3/2}}$ and the corresponding orbital/heat magnetic moments $m_{\pm}\left(\boldsymbol{k}\right) = \frac{-\lambda^{2}\Delta}{2(\Delta^{2}+k^{2}\lambda^{2})}$ and $m_{\pm}^{E}\left(\boldsymbol{k}\right) =$ $\frac{\pm \lambda^2 \Delta}{(\Delta^2 + k^2 \lambda^2)^{1/2}}$ (The real parts of quantum geometric tensors are given in Supplemental Material [35]). shown in Fig. 2(b), $m_n^E(\mathbf{k})$ exhibits a smooth distribution in momentum space than $m_{\pm}(\mathbf{k})$ and $\Omega_{n}(\mathbf{k})$. In the strong-exchange field limit $(\overline{\Delta}^2 \gg k^2 \lambda^2)$, the orbital/heat magnetic moments reduce to be $m_{\pm}\left(\boldsymbol{k}\right)$ \approx $-\frac{\lambda^2}{2\Delta}\left(1-k^2\lambda^2/\Delta^2\right)$ and $m_{\pm}^E(\mathbf{k})\approx\pm\lambda^2\left(1-k^2\lambda^2/2\Delta^2\right)$. Clearly, the Rashba SOC plays a primary role in the circular phonon dichroisms.

With the aid of Eq. (4), we could calculate the circular phonon dichroism when q is along $\arctan(q_y/q_x) = \pi/4$ direction and depict the results in Fig. 3. There are

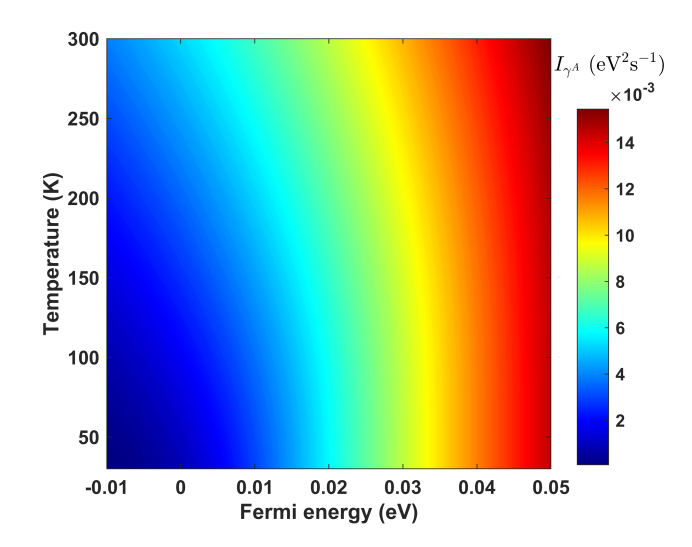


Figure 4. Temperature- and Fermi energy- dependence of the integration of the circular phonon dichroism of Rashba 2DEG with $q/k_{Fmin} = 0.04$.

several salient features in $\gamma^{R/L}$. First, in the longwavelength region (small q), the absorptions of the rightand left-hand circularly polarized phonons are strong but almost identical, implying a vanishing circular phonon dichroism. Second, as the phonon wave-vector increases, the difference of absorption coefficients between oppositely circularly polarized phonons becomes pronounced at $q/k_{Fmin} \sim 1.2$ and forms a two-peak structure as shown in Figs. 3(a)-(c). Third, Fig. 3(d) shows the interband electron-hole pair excitations between states with opposite spins induced by phonons (labeled by q_2) and q_3) are dominant in $\gamma^L - \gamma^R$, similar to the 3D Weyl semimetals [34]. The intraband contribution instead causes a global change of the absorption coefficients. Furthermore, we find the double peaks mainly originate from the asymmetry of interband electron-hole pair excitations in the two regions near the Fermi surface. In addition, we could evaluate the related circular phonon dichroism and have $(\gamma^L - \gamma^R)/\bar{c} \sim 10/\text{m}$, where $\bar{c} = (c_l + c_t)/2 \approx 10^3 \text{m/s}$ is the average sound velocity. Noted that, in our numerical calculations, we focus on the acoustic phonons and choose $c_{l/t}$ as the order of 10^3m/s throughout this work.

We also calculate the f-sum rule integration of the circular phonon dichroism in Eq. (13) of the Rashba 2DEG and depict the dependence of temperature and Fermi energy of I_{γ^A} in Fig. 4. It is clear that, as temperature or the Fermi level increases, the circular phonon dichroism gets greatly stronger due to the enhancement of population of phonon induced electron-hole excitations.

Let us briefly discuss the experimental detection of phonon dichroisms. The difference of absorption between the left and right circularly polarized phonons can be accessed by the pulse-echo ultrasound technique [62], whereas the phonon polarization of linearly polarized acoustic waves can be detected by Raman spectroscopy [63]. Recently, interface-specific nonlinear optical technique has been used to probe the polaronic signature in LaAlO₃/SrTiO₃ interface [64], providing a feasible platform to detect the quantum-geometry modified phonon dichroism therein. Very recently, the circular dichroism of phonon has been reported in a magnetic Weyl semimetal [65, 66] and makes the present predictions be tested experimentally. It should be emphasized that together with the spin- and angle-resolved circular dichroism photoemission spectroscopy [31], the phonon dichroisms allow us to extract the complete information of all of six quantum geometric quantities (in Table. I) of electrons in solids.

Conclusions.--We established the deep connection between phonon dichroisms and the unusual quantum geometry of electron bands in noncentrosymmetric magnetic metals. Notably, we found that the circular phonon dichroism is directly related to the HMM of electrons through the sum rule. The key results are examined in the typical Rashba 2DEG and can be accessible by various spectroscopy techniques. Our findings provide a novel contact-free acoustic method for detecting the fundamental quantum geometry in particular the HMM of electrons. It would inspire the investigation of the quantum geometry effect on the fascinating quantum phenomena in other coupled systems among electron and bosonic excitations in a large variety of quantum materials.

The authors thank D.-H. Liu, W.-Y. Shan, J.-R. Shi and Y.-H. Zhang for useful discussions. This work was financially supported by the National Key R&D Program of the MOST of China (Grant No. 2024YFA1611300), the National Natural Science Foundation of China (Grant No. 12574059 and No. 12174394), HFIPS Director's Fund (Grant No. BJPY2023B05), Anhui Provincial Major S&T Project (s202305a12020005) and the Basic Research Program of the Chinese Academy of Sciences Based on Major Scientific Infrastructures (Grant No. JZHKYPT-2021-08) and the High Magnetic Field Laboratory of Anhui Province under Contract No. AHHM-FX-2020-02.

- * Both authors contribute equally to this work.
- † taoqin@ahu.edu.cn
- [‡] jhzhou@hmfl.ac.cn
- § ygyao@bit.edu.cn
- [1] J. P. Provost and G. Vallee, Communications in Mathematical Physics **76**, 289 (1980).
- [2] F. Wilczek and A. Shapere, Geometric Phases in Physics (WORLD SCIENTIFIC, 1989).
- [3] P. Törmä, Phys. Rev. Lett. **131**, 240001 (2023).
- [4] D. Xiao, M.-C. Chang, and Q. Niu, Rev. Mod. Phys. 82, 1959 (2010).

- [5] N. Nagaosa, J. Sinova, S. Onoda, A. H. MacDonald, and N. P. Ong, Rev. Mod. Phys. 82, 1539 (2010).
- [6] M. Z. Hasan and C. L. Kane, Rev. Mod. Phys. 82, 3045 (2010).
- [7] X.-L. Qi and S.-C. Zhang, Rev. Mod. Phys. 83, 1057 (2011).
- [8] N. P. Armitage, E. J. Mele, and A. Vishwanath, Rev. Mod. Phys. 90, 015001 (2018).
- [9] Y.-Q. Ma, S. Chen, H. Fan, and W.-M. Liu, Phys. Rev. B 81, 245129 (2010).
- [10] L. Liang, T. I. Vanhala, S. Peotta, T. Siro, A. Harju, and P. Törmä, Phys. Rev. B 95, 024515 (2017).
- [11] L. Liang, S. Peotta, A. Harju, and P. Törmä, Phys. Rev. B 96, 064511 (2017).
- [12] S. Sengupta, M. N. Y. Lhachemi, and I. Garate, Phys. Rev. Lett. 125, 146402 (2020).
- [13] L.-H. Hu, J. Yu, I. Garate, and C.-X. Liu, Phys. Rev. Lett. 127, 125901 (2021).
- [14] Y. Ren, C. Xiao, D. Saparov, and Q. Niu, Phys. Rev. Lett. 127, 186403 (2021).
- [15] Z. Wang, L. Dong, C. Xiao, and Q. Niu, Phys. Rev. Lett. 126, 187001 (2021).
- [16] P. Törmä, S. Peotta, and B. A. Bernevig, Nature Reviews Physics 4, 528 (2022).
- [17] S. A. Chen and K. T. Law, Phys. Rev. Lett. 132, 026002 (2024).
- [18] J.-L. Zhang, W. Chen, H.-T. Liu, Y. Li, Z. Wang, and W. Huang, Phys. Rev. Lett. 132, 136001 (2024).
- [19] Y. Gao, S. A. Yang, and Q. Niu, Phys. Rev. Lett. 112, 166601 (2014).
- [20] I. Sodemann and L. Fu, Phys. Rev. Lett. 115, 216806 (2015).
- [21] A. Gao, Y.-F. Liu, J.-X. Qiu, B. Ghosh, T. V. Trevisan, Y. Onishi, C. Hu, T. Qian, H.-J. Tien, S.-W. Chen, M. Huang, D. Bérubé, H. Li, C. Tzschaschel, T. Dinh, Z. Sun, S.-C. Ho, S.-W. Lien, B. Singh, K. Watanabe, T. Taniguchi, D. C. Bell, H. Lin, T.-R. Chang, C. R. Du, A. Bansil, L. Fu, N. Ni, P. P. Orth, Q. Ma, and S.-Y. Xu, Science 381, 181 (2023).
- [22] J. Yu, C. J. Ciccarino, R. Bianco, I. Errea, P. Narang, and B. A. Bernevig, Nature Physics 20, 1262 (2024).
- [23] J. Hu, W. Li, H. Wang, and K. Chang, arXiv:2410.09677.
- [24] D. Xiao, J. Shi, and Q. Niu, Phys. Rev. Lett. 95, 137204 (2005).
- [25] T. Thonhauser, D. Ceresoli, D. Vanderbilt, and R. Resta, Phys. Rev. Lett. 95, 137205 (2005).
- [26] T. Qin, Q. Niu, and J. Shi, Phys. Rev. Lett. 107, 236601 (2011).
- [27] D. Y. Smith, Phys. Rev. B 13, 5303 (1976).
- [28] B. T. Thole, P. Carra, F. Sette, and G. van der Laan, Phys. Rev. Lett. 68, 1943 (1992).
- [29] I. Souza and D. Vanderbilt, Phys. Rev. B 77, 054438 (2008).
- [30] W. Yao, D. Xiao, and Q. Niu, Phys. Rev. B 77, 235406 (2008).
- [31] M. Kang, S. Kim, Y. Qian, P. M. Neves, L. Ye, J. Jung, D. Puntel, F. Mazzola, S. Fang, C. Jozwiak, A. Bostwick, E. Rotenberg, J. Fuji, I. Vobornik, J.-H. Park, J. G. Checkelsky, B.-J. Yang, and R. Comin, Nature Physics 21, 110 (2025).
- [32] S.-K. Bac, F. Le Mardelé, J. Wang, M. Ozerov, K. Yoshimura, I. Mohelský, X. Sun, B. A. Piot, S. Wimmer, A. Ney, T. Orlova, M. Zhukovskyi, G. Bauer, G. Springholz, X. Liu, M. Orlita, K. Park, Y.-T. Hsu,

- and B. A. Assaf, Phys. Rev. Lett. 134, 016601 (2025).
- [33] S. Kim, Y. Chung, Y. Qian, S. Park, C. Jozwiak, E. Rotenberg, A. Bostwick, K. S. Kim, and B.-J. Yang, Science 388, 1050 (2025).
- [34] D. Liu and J. Shi, Phys. Rev. Lett. 119, 075301 (2017).
- [35] See Supplemental Material for details of the electronphonon interaction, the force operator, the six quantum geometric tensors, calculations of the quantum geometric factor, the linear and circular phonon dichroism coefficients and the sum rule for the thermal transport.
- [36] W.-Y. Shan, Phys. Rev. B 105, L121302 (2022).
- [37] A. H. Castro Neto, F. Guinea, N. M. R. Peres, K. S. Novoselov, and A. K. Geim, Rev. Mod. Phys. 81, 109 (2009).
- [38] D. Xiao, G.-B. Liu, W. Feng, X. Xu, and W. Yao, Phys. Rev. Lett. 108, 196802 (2012).
- [39] T. Cao, G. Wang, W. Han, H. Ye, C. Zhu, J. Shi, Q. Niu, P. Tan, E. Wang, B. Liu, and J. Feng, Nature Communications 3, 887 (2012).
- [40] Y. A. Bychkov and E. I. Rashba, JETP Lett 39, 78 (1984).
- [41] J. Zhou, W.-Y. Shan, and D. Xiao, Phys. Rev. B 91, 241302 (2015).
- [42] X. Wan, A. M. Turner, A. Vishwanath, and S. Y. Savrasov, Phys. Rev. B 83, 205101 (2011).
- [43] W.-K. Tse and A. H. MacDonald, Phys. Rev. Lett. 105, 057401 (2010).
- [44] T. Liu, X.-B. Qiang, H.-Z. Lu, and X. C. Xie, National Science Review 12, nwae334 (2024).
- [45] W. Kohn, Phys. Rev. 133, A171 (1964).
- [46] R. Resta, Journal of Physics: Condensed Matter 30, 414001 (2018).
- [47] B. S. Shastry, Phys. Rev. B 73, 085117 (2006).
- [48] M. Barkeshli, S. B. Chung, and X.-L. Qi, Phys. Rev. B 85, 245107 (2012).
- [49] T. L. Hughes, R. G. Leigh, and E. Fradkin, Phys. Rev. Lett. 107, 075502 (2011).
- [50] H. Shapourian, T. L. Hughes, and S. Ryu, Phys. Rev. B 92, 165131 (2015).
- [51] C. Kittel, Quantum theory of solids, 2nd ed. (Wiley, New York, 1987).
- [52] D. Pines and P. Nozières, The Theory of Quantum Liquids: Normal Fermi liquids, Advanced book classics

- (W.A. Benjamin, New York, 1966).
- [53] Since the acoustic phonon energy is typically much smaller than the Fermi energy, the initial and final states of the electron should be close to the Fermi surface during phonon absorption. Further taking into account the spin-orbit coupling, the spin-momentum locking of electrons could affect the phonon behaviors through the electron-phonon interaction.
- [54] The generalization of the sum rule and a procedure to extract the electron heat and orbital magnetic moments from the experimental measurements on phonon dichroism are also discussed [35].
- [55] G. van der Laan and A. I. Figueroa, Coordination Chemistry Reviews 277-278, 95 (2014).
- [56] A. Ohtomo and H. Y. Hwang, Nature **427**, 423 (2004).
- [57] C. Liu, X. Yan, D. Jin, Y. Ma, H.-W. Hsiao, Y. Lin, T. M. Bretz-Sullivan, X. Zhou, J. Pearson, B. Fisher, J. S. Jiang, W. Han, J.-M. Zuo, J. Wen, D. D. Fong, J. Sun, H. Zhou, and A. Bhattacharya, Science 371, 716 (2021).
- [58] D. Culcer, A. MacDonald, and Q. Niu, Phys. Rev. B 68, 045327 (2003).
- [59] A. El Hamdi, J.-Y. Chauleau, M. Boselli, C. Thibault, C. Gorini, A. Smogunov, C. Barreteau, S. Gariglio, J.-M. Triscone, and M. Viret, Nature Physics 19, 1855 (2023).
- [60] X. Li, W. V. Liu, and L. Balents, Phys. Rev. Lett. 112, 067202 (2014).
- [61] L. P. Gor'kov and E. I. Rashba, Phys. Rev. Lett. 87, 037004 (2001).
- [62] B. Lüthi, *Physical acoustics in the solid state* (Springer Berlin, Heidelberg, 2006).
- [63] C. Faugeras, M. Amado, P. Kossacki, M. Orlita, M. Kühne, A. A. L. Nicolet, Y. I. Latyshev, and M. Potemski, Phys. Rev. Lett. 107, 036807 (2011).
- [64] X. Liu, T. Zhou, Z. Qin, C. Ma, F. Lu, T. Liu, J. Li, S.-H. Wei, G. Cheng, and W.-T. Liu, Science Advances 9, eadg7037 (2023).
- [65] R. Yang, Y.-Y. Zhu, M. Steigleder, Y.-C. Liu, C.-C. Liu, X.-G. Qiu, T. Zhang, and M. Dressel, Phys. Rev. Lett. 134, 196905 (2025).
- [66] M. Che, J. Liang, Y. Cui, H. Li, B. Lu, W. Sang, X. Li, X. Dong, L. Zhao, S. Zhang, T. Sun, W. Jiang, E. Liu, F. Jin, T. Zhang, and L. Yang, Phys. Rev. Lett. 134, 196906 (2025).